Research article

Force attenuation performance in sandwich structures with STF and M-STF encapsulation

Mohammad Rauf Sheikhi [a,b,c], Kenan Bayrak [d], Esra Ozdemir [e], Selim Gürgen [f,*]

[a] *The State Key Laboratory of Heavy-duty and Express High-power Electric Locomotive, Changsha, 410075, China*
[b] *Key Laboratory of Traffic Safety on Track of Ministry of Education, School of Traffic & Transportation Engineering, Central South University, Changsha, 410075, China*
[c] *National & Local Joint Engineering Research Center of Safety Technology for Rail Vehicle, Changsha, 410075, China*
[d] *Department of Aviation Science and Technology, Eskişehir Osmangazi University, Eskişehir, Turkey*
[e] *Turkish Aerospace Industries Inc., Ankara, Turkey*
[f] *Department of Aeronautical Engineering, Eskişehir Osmangazi University, Eskişehir, Turkey*

A B S T R A C T

In this study, we investigate the role of adding shear thickening fluids (STFs) and multi-functional shear thickening fluids (M-STFs) to the core of a sandwich-structured composite made of aluminum facesheets and XPS foam cores with different geometries on force attenuation performance. Six different core designs were machined, and all designs had the same space for adding STFs and M-STFs. STF with 40 wt% SiO_2 in PEG 400 was selected and fabricated. M-STFs were made by adding multi-walled carbon nanotubes (MWCNTs) up to 1.5 wt%. The effects of MWCNTs on the rheological and electrical properties of the STF were investigated. The force attenuation tests were performed with an impact drop tower test system at three different heights with 5, 10, and 15 J energy levels. According to the results, V6_STF (with 16 holes with a diameter of 6 mm) and H6_STF (with 16 rectangular cubic column with cross-sections of 6×6 mm) designed sandwich structures showed better performance in terms of force attenuation compared with the other samples. Next, these two sandwich structures were filled again with M-STF (0.5 wt% MWCNT), and the force attenuation performance of the structures showed an improvement further, and the H6_STF_CNT sample improved by 24.8% compared to the clean sandwich structure sample. These results demonstrate the potential of STFs and M-STFs in strengthening the force attenuation performance of sandwich structures with XPS foam cores, mainly when used with appropriate core geometry.

1. Introduction

Sandwich-structured composite has been widely employed in various applications due to its high strength-to-weight ratio. These structures comprise two stiff exterior face sheets (composites, aluminum, etc.) with a lightweight core material (foam, honeycomb, or corrugated sheets, etc.) sandwiched between them [1]. The core material plays a critical role in determining the mechanical properties of the sandwich structure [2]. Therefore, improving the core design can significantly enhance the overall performance of the sandwich structure [3]. Many studies have examined the effect of different core materials, such as aluminum, copper, wood, cork, metal, and

---

polymer foam, on the structural performance of the sandwich structures [4,5]. For sandwich structures, geometrical design parameters of the core layer play an essential role in fatigue and energy absorption (EA) applications [6].

Multifunctionality is crucial in some specific sandwich-structured composites as it integrates multiple properties into a single lightweight composite material. Sandwich structures can be designed to provide functions such as increased stiffness and strength, thermal and acoustic insulation, vibration damping, fire, impact resistance, and more. This can lead to weight reduction, cost savings, enhanced safety, and improved performance of structures, making them a versatile candidate for a wide range of applications [7,8]. Applying smart materials to the sandwich-composite structures is a promising method for making multifunctional structure. Shear thickening fluids (STFs) are one of the innovative materials that can be used for this purpose.

STFs are complex fluids with increasing viscosity when subjected to shear stress, making them more challenging to flow under different mechanical forces (impact and vibration). This phenomenon results from the creation of transient particle networks within the fluid, which can induce an abrupt increase in viscosity when the particles collide [9]. STFs could be utilized in various fields like body armor and sporting gear because of their capacity to offer impact resistance and absorb shocks [10]. The ability of STFs to increase viscosity under stress is influenced by the characteristics of the dispersed phase and medium, as well as the presence of additives [11]. By incorporating conductive fillers, such as carbon nanotubes (CNT), carbon nanofiber (CNF), graphene, or carbon black (CB), or using ionic liquids [12] as dispersants [13–17], the STFs exhibit both enhanced shear-thickening (ST) performance and electrical conductivity [18]. These types of multifunctional STFs can improve electrical and mechanical responses in intelligent systems [19,20]. Besides STF, shear stiffening gels (SSGs) are another non-Newtonian-based innovative material that can be used in anti-impact applications. High molecular weight polymers with stiffening characteristics in modulus are known as SSGs. SSGs exhibit ST effect through phase transitions due to chemical cross-links (dynamic weak boron-oxygen cross-links) [21–23]. STFs and SSGs have distinct compositions, processes, and properties, but both exhibit excellent ST behaviors.

Many studies show STF applications for low- and high-velocity impact resistance [24–31], stab resistance [32–34], explosion resistance [35–38], vibration control [39–45], adaptive structure [46–48], and industrial polishing [49–51] which indicates the capability of STF for different protective applications. Sheikhi et al. [29] have studied multilayer sandwich structures consisting of foam, cork, and wrap-knitted spacer fabrics. STF was infused within foam layers, and multi-layer arrangements were devised for anti-impact structures. They determined that the most efficient design for specific energy absorption includes a 20 mm coarse-granule cork layer followed by a foam layer and a WKSF layer from top to bottom. In addition, maximum reaction forces and energy-absorbing capacity increase with the contribution of STF layers for all structures. Zhao et al. [52] investigated the interactions between five different fluids and PU skeletons (two different moduli) during low-velocity impact. In contrast to Newtonian fluids, the thickening gradient of non-Newtonian fluids can distribute the impact stress horizontally and exhibit a more robust interaction with the skeleton, generating regions of low stress within the composite and enhancing impact resistance. The lower modulus of the PU skeleton allows for increased transverse deformation, thereby promoting greater energy exchange between the fluid and solid materials during impact, enhancing impact resistance performance. Caglayan et al. [53] incorporated STF into closed-cell PU foam. The experimental findings from sandwich composites reveal that PU foam cores filled with STF demonstrate a higher energy absorption rate than their pure counterparts. The impact energy absorption capacity of STF-integrated PU foam cores grows due to higher thickness-to-length ratios and increased cell densities obtained through the STF integration.

Wu et al. [54] studied the dynamic compressive properties of structures featuring pyramidal lattice truss cores filled with STF at high strain rates. The research indicates that the strength reached at the buckling of core beams, once filled with STF, is nearly three times greater than that of empty truss cores. Chatterjee et al. [55] investigated the anti-ballistic response of STF-filled 3D-mat-Kevlar sandwich composites. The researchers discovered that the sandwich composite panels incorporating STF could absorb 96.3% of the incident energy, representing a 67.4% increase in energy absorption compared to hollow sandwich composite panels. Fu et al. [25] have integrated styrene/acrylate particle-based STF in a carbon fiber-honeycomb sandwich composite structure with two different core thicknesses. The study shows that EA in thin core sandwich structures filled with STF have almost double times higher under low-velocity impact tests and has less penetration depth than an aluminum foam. Gürgen et al. [56] investigated different layer
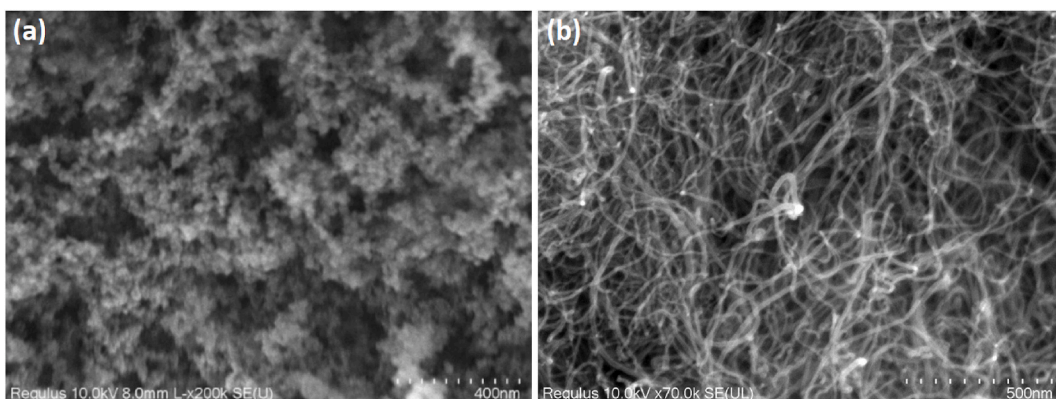

Fig. 1. SEM images for (a) silica and (b) MWCNT.

configurations in the composite structure formed with cork plate and STF. The study shows that a structures with 10 layers performed the best result at low-velocity impact test at 5J energy level. Also, multilayer structures can become more effective in energy dissipation at low-velocity impacts.

Based on the literature survey, previous studies on sandwich structures have primarily concentrated on improving anti-impact performance through STF and MWCNT-reinforced STF. At the same time, the geometry design of the core layer for adding STFs and M-STFs has received limited exploration. To overcome this constraint and further enhance the anti-impact properties of sandwich structures, this work focuses on force attenuation (FA) performance with various core geometrical designs for adding STFs and multifunctional shear thickening fluids (M-STFs).

2. Experimental details

2.1. STF and M-STF preparation

STF was fabricated by distributing 20 nm particle size fumed silica (SiO_2) (Aerosil 90, Evonik, Germany) in a 400 g/mol polyethylene glycol (PEG, $C_2nH_4n+2On+1$) medium (81,172, Sigma-Aldrich, USA). Scanning electron microscopy (SEM) images of silica and MWCNT are shown in Fig. 1a and b, respectively. These images can help visualize the network structure and provide insights into the particle-particle interactions contributing to ST behavior.

The STF fabrication included the stepwise addition of SiO_2 to PEG while homogenizing the suspension for 1 h using a high-speed homogenizer (T25, IKA, Germany). The SiO_2 fraction of the STF remained at 40% wt. as recommended by Caglayan et al. [53] for optimum ST performance. After the STF fabrication, MWCNT (8–10 nm, Nanografi, Turkey) was added to the suspension at concentrations of 0.50, 1.00, and 1.50 wt% and mixed for 30 min. Rheological and electrical testing was carried out on the suspensions after 2 h of preparation.

2.2. Manufacturing of sandwich structures

The sandwich structures were constructed using facesheets made of 1.6 mm thick 7075 aluminum series and an 18 mm thick closed cell extruded polystyrene foam (XPS) with a 35 kg/m^3 density as the core material. XPS is a rigid foam composed of polystyrene polymer. It is made by extruding molten polystyrene through a die, which results in a closed-cell structure. XPS foam has good thermal properties, muscular compressive strength, and resistance to moisture absorption [57]. To fill STFs and M-STFs, 6 different geometries were machined into XPS foam core layers. Core designs had the same amount of space for restocking STFs and M-STFs. These designs were based on two main basic concepts. The first one was made to drill holes of three different diameters in the form of cylindrical geometry. The other design is rectangular channels that were opened on the top surface of the core material. The grooving operations on XPS foam material were performed using a CNC Milling machine. STF and M-STF suspensions were injected into the core layers using a syringe. The facesheets and XPS core were assembled using a tape adhesive by Beta Kimya, Turkey. Fig. 2 shows the sandwich structures, and Table 1 presents the dimension parameters of core designs. Table 2 gives the design of the experiments.
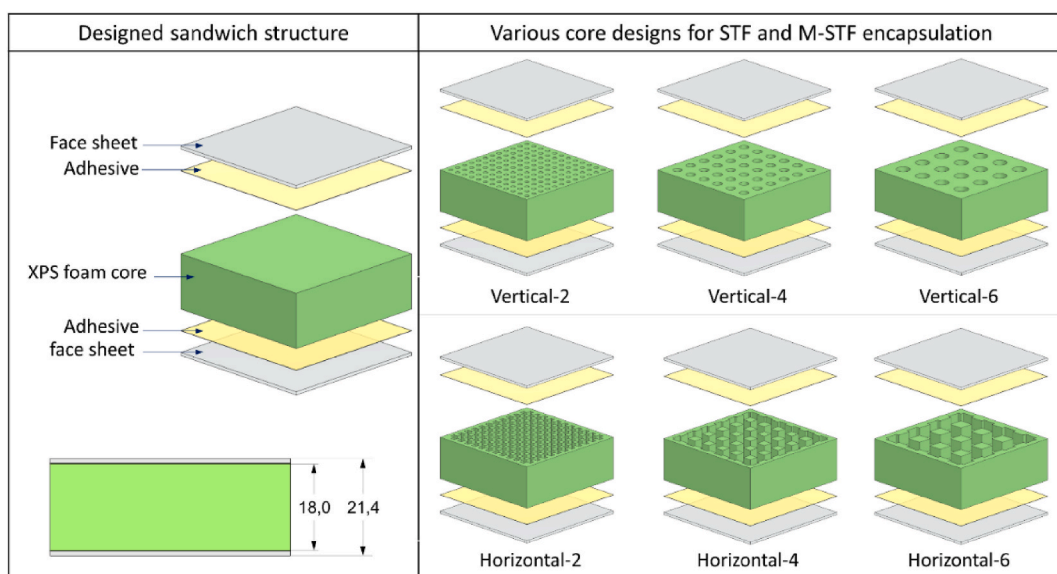

Fig. 2. Designed sandwich structures.

Table 1
Dimensional parameters for core designs.

Specimen	Hole/channel width	Hole/channel depth	Number of holes/channels
Vertical-2	Ø 2.0 mm	18.0 mm	144
Vertical-4	Ø 4.0 mm	18.0 mm	36
Vertical-6	Ø 6.0 mm	18.0 mm	16
Horizontal-2	2.0 mm	5.29 mm	11×11
Horizontal-4	4.0 mm	5.14 mm	6×6
Horizontal-6	6.0 mm	4.99 mm	4×4

Table 2
Design of the experiments.

Specimen code	Description
Neat	Neat sandwich structure
V2_STF	Sandwich structure with STF - Core Pattern Vertical-2
V4_STF	Sandwich structure with STF - Core Pattern Vertical-4
V6_STF	Sandwich structure with STF - Core Pattern Vertical-6
H2_STF	Sandwich structure with STF - Core Pattern Horizontal-2
H4_STF	Sandwich structure with STF - Core Pattern Horizontal-4
H6_STF	Sandwich structure with STF - Core Pattern Horizontal-6
V6_STF_CNT	Sandwich structure with STF/0.5%MWCNT - Core Pattern Vertical-6
H6_STF_CNT	Sandwich structure with STF/0.5%MWCNT - Core Pattern Horizontal-6

2.3. FA test setup

In this study, sandwich structures were investigated in a drop tower, as shown in Fig. 3. The impactor utilized in the experiment possessed a hemispherical shape with a diameter of 15 mm and weighed 1.024 kg. Drop tests were conducted on each specimen at 5, 10, and 15 J energy levels. The impactor was released from heights corresponding to the energy above levels, and the FA of the impact was measured using a dynamometer positioned beneath the specimens.

2.4. Rheological and electrical resistance measurements

Rheological tests were conducted in an Anton Paar MCR 302 rheometer equipped with a 25 mm diameter standard parallel plate system. A gap of 1 mm was used between the plates, and a range of shear rates from 0 to 1000 s^{-1} was employed in the testing. All the tests were carried out at a temperature of 25 °C. Electrical resistance measurements were carried out using a UNIT UT90A multimeter.
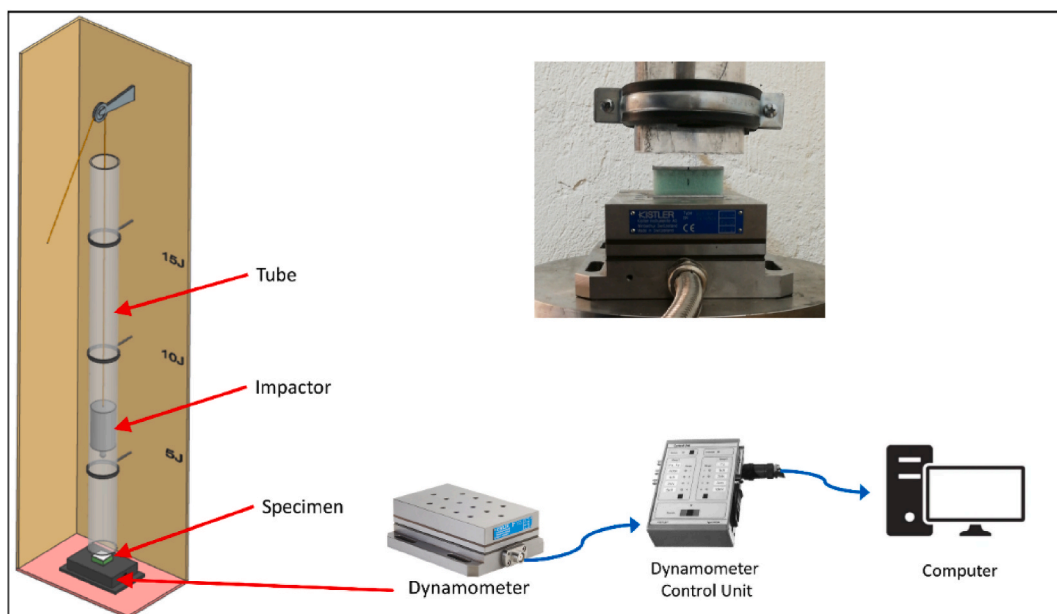

Fig. 3. Drop tower based FA test setup.

To ensure consistent and standardized measurements, all samples were fixed and handled at identical conditions, with the probes positioned 40 mm apart and penetrating 5 mm into the mixture. Furthermore, a weight of 50 g of STFs/M-STFs was used in a 50 mm diameter beaker.

3. Results and discussion

3.1. Rheological properties of STF and M-STFs

The study analyzed the rheology of STFs and M-STFs having various amounts of MWCNTs at concentrations of 0.5 and 1 wt%. The viscosity of these materials was evaluated for shear rate, and the results are shown in Fig. 4, which presents the changes in viscosity of STF and M-STFs at room temperature. The rheological results presented in the study highlight the behavior of STFs and M-STFs with and without the addition of MWCNTs. The results show that the incorporation of silica particles into PEG leads to ST, with the mixture's viscosity increasing as the shear rate increases. This behavior is typical of STFs, characterized by a non-Newtonian response, and their viscosity changes with the shear rate or shear stress.

Adding MWCNTs to STFs leads to a considerable enhancement in the initial and maximum viscosities of the M-STFs, with a corresponding reduction in the critical shear rate required for ST to occur. Results show that the M-STF with 1.0 wt% MWCNT leads the highest peak viscosity of 3576 Pa s, which is a significant improves compared to the clean STFs and M-STFs containing 0.5 wt% MWCNT. The critical thickening rate at which the maximum viscosity is defined also shifts to lower shear rates with increased MWCNT. This indicates that adding MWCNTs in STFs enhances their ST behavior and is consistent with previous studies [18,41,58]. Furthermore, it is worth noting that the test for the M-STF with 1.0 wt% MWCNT terminates at a shear rate of 10 s^{-1} due to the specified force limit of the rheometer. For M-STF containing more than 1.0 wt% MWCNT, the suspension nearly transitions into the solid phase, indicating a significant level of solid-like behavior. This observation highlights the considerable influence of MWCNTs on the M-STF rheology, where a higher concentration of MWCNTs leads to a more significant amount of ST and a more solid-like behavior. Adding MWCNTs to STFs can significantly enhance their performance, making them more suitable for a wide range of applications, including the core of the sandwich structures. The results also demonstrate the importance of carefully controlling the concentration of MWCNTs in the STFs to achieve optimal performance.

3.2. Electrical resistance of M-STFs

MWCNTs are known to be highly conductive due to their unique one-dimensional structure, which provides efficient pathways for electron transport [59]. When MWCNTs are dispersed in a liquid medium, such as an STF suspension, they can form a conductive network that allows electrons to flow through the suspension [60]. This can significantly reduce the electrical resistance of the suspension. As more MWCNTs are added to the suspension, the conductivity of the network increases, resulting in a decrease in electrical resistance. However, there is a critical point where the MWCNTs form a continuous conductive network that spans the suspension's entire volume, known as the percolation threshold. Below this threshold, the conductivity of the suspension is low, and above this threshold, the conductivity increases rapidly. The percolation threshold is affected by multiple factors, including the shape, size, and concentration of the conductive particles, as well as the properties of the liquid medium [61,62]. Fig. 5 illustrates the electrical resistance of M-STFs plotted against the MWCNT content. In this case, the percolation threshold for MWCNTs in the STF suspension was between 0.2 and 0.4 wt% based on the electrical resistance measurements. This means that adding less than 0.2 wt% MWCNTs to the STF suspension would not significantly reduce the electrical resistance, and adding more than 0.4 wt% would not significantly increase the conductivity. It is also noteworthy that increasing the amount of MWCNTs in the suspension can increase the inert viscosity of the STF suspension. This is because MWCNTs tend to form agglomerates, which can increase the viscosity of the suspension.
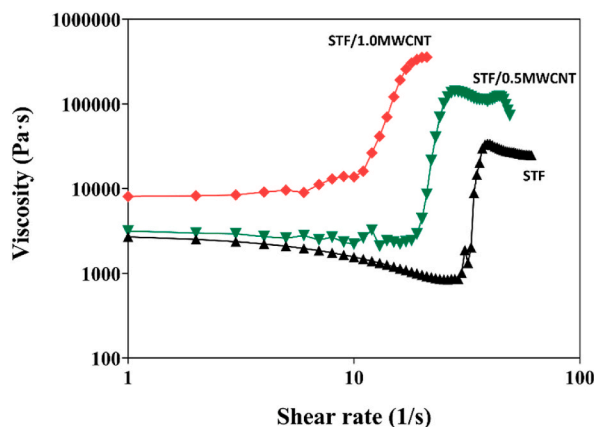

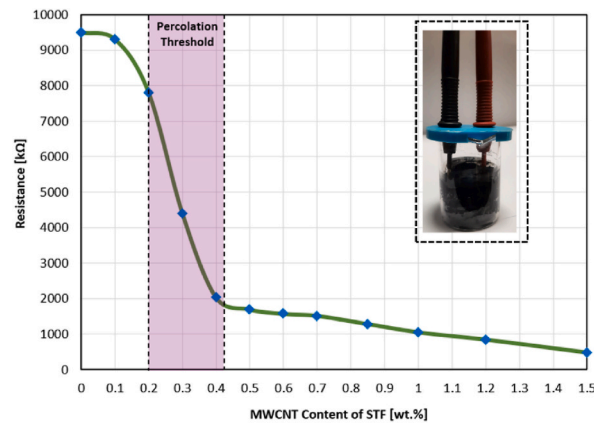**Fig. 4.** Rheological behavior of STF and M-STFs.

Fig. 5. The electrical resistance of M-STFs as a function of MWCNT content.

Therefore, there is a trade-off between achieving high conductivity and maintaining low viscosity in the STF suspension, which needs to be carefully balanced.

3.3. FA performance of sandwich structures

Fig. 6 represents the peak reaction curves of designed Neat, V6_STF, H6_STF, V6_STF_CNT, and H6_STF_CNT sandwich structures in impact energy of 15 J. These plots show the maximum reaction force (MRF) values, based on force (N), over time (s). The MRF curves are necessary because they show how much force the sandwich structures can withstand and dissipate during the impact. The lower the MRF, the better the FA performance. This means the sandwich structure can protect the underlying material or object from damage by dissipating and absorbing the impact energy. The first peak of the peak reaction curve represents the MRF after the first collision of the impactor. This peak reflects the initial response of the structure to the impact. The properties of the aluminum facesheets, the XPS core, and the STF and M-STFs influence the first peak. The STF and M-STFs provide ST behavior, which increases the viscosity and resistance of the core in impact event time. The ST behavior of the STF or M-STF depends on the particle size, concentration, and distribution of PEG and the SiO_2 and MWCNTs solid particles. The lower the MRF of the first peak, the more influential the sandwich structure is in reducing the FA.

The peak reaction curves are obtained for all of the designed sandwich structures, and MRFs of the first collision impact are presented in Fig. 7. V6_STF and H6_STF designed sandwich structures show the best performance in reducing FA. This can be associated with higher amounts of STF in each cylindrical hole and rectangular channel in V_STF and H_STF designs, respectively.
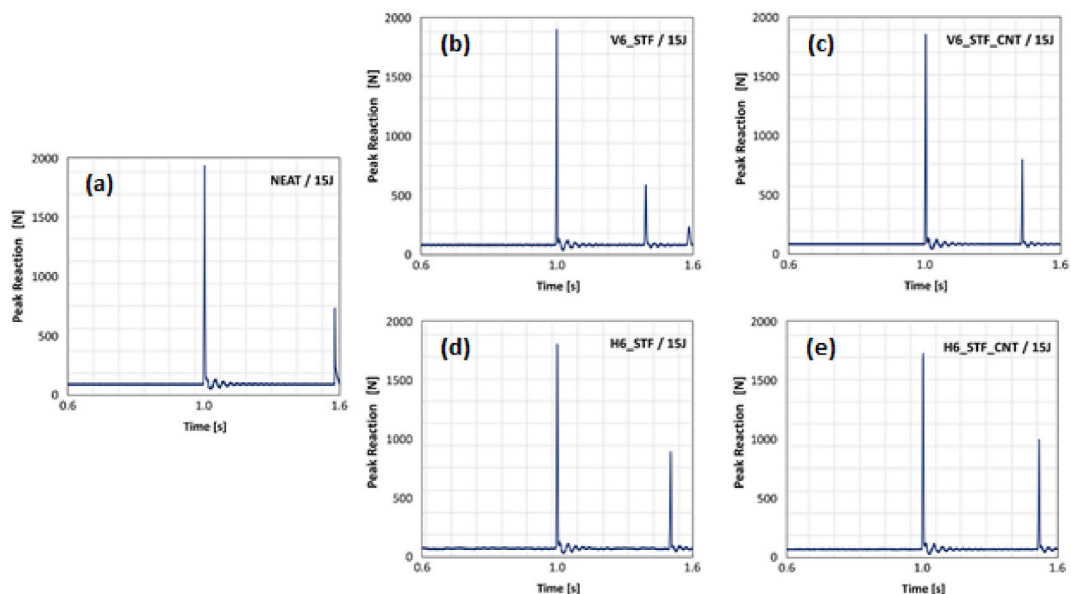

Fig. 6. Peak reaction forces for (a) Neat, (b) V6_STF, (c) V6_STF_CNT, (d) H6_STF, and (e) H6_STF_CNT under 15 J impact.
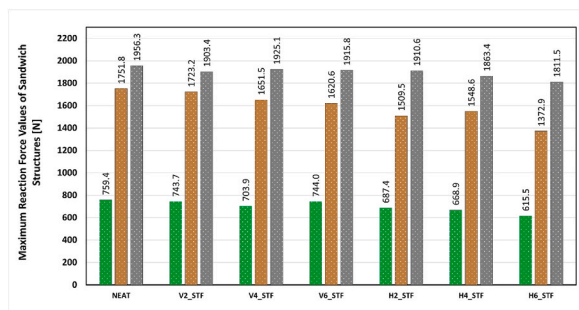
Fig. 7. Maximum reaction forces of designed sandwich structures filled with STF.

Considering the individual STF pockets in V6_STF and H6_STF specimens, STF gets thickened in bulk form upon loading, leading to the contribution of a higher volume of fluid rather than the viscosity increase in tiny drops of STF in distinct locations of the specimens. On the other hand, ST effect in smaller cavities may be limited to suppressing the impact forces, thereby falling behind the specimens with larger cavities in terms of force attenuation. We know that STF has the property of increasing viscosity with increasing shear rate. Therefore, when the sandwich structure is subjected to impact, the STF in the core layer undergoes ST, which increases the deformation resistance of the core layer and reduces the transmitted force to the aluminum back face.

As seen in Fig. 8, after adding MWCNTs in STF, the performance of FA is further improved. In section 3.1, we observed that MWCNTs can increase the ST rheology. Also, MWCNTs have a strong adsorption capacity on SiO_2 nanoparticles, which are the main components of silica-based STF. It can form a new bond containing MWCNT in STF, which increases the contact force and interparticle friction under shear, viscosity, and a critical shear rate. STF can have a more substantial ST effect at lower shear strain than STF. M-STF is fabricated of both STF and MWCNTs, which can create a network-like structure inside the STF matrix. This network considerably improves the STF's EA capabilities, improving FA performance in V6_STF_CNT and H6_STF_CNT sandwich structures. Moreover, MWCNTs in M-STFs play as reinforcing fillers, improving the mechanical characteristics of the STF matrix. This enhances the STF's viscosity and makes it more resistant to deformation under applied stresses, resulting in better FA performance.

Consequently, the V6_STF_CNT and H6_STF_CNT sandwich structures with various core geometrical designs showed significant improvement in FA performance compared to neat sandwich structures. The improvement was up to 24.9% for the H6_STF_CNT design. Fig. 9 shows the FA performance of M-STF-based sandwich structures (V6_STF_CNT and H6_STF_CNT) compared with the neat sample.

Fig. 10 shows the deformation properties before and after the impact of Neat, H6_STF, and H6_STF_CNT designed sandwich structures at 15 J impact energy. Their deformations are related to the mechanical properties of the XPS foam core and the STFs or M-STFs that are added to it. In the Neat XPS sandwich structure (Fig. 10a), the XPS foam core did not disintegrate and was only compressed because it did not contain any STFs or M-STFs that could increase its viscosity and stiffness under impact. The XPS foam core could deform and recover its shape to some extent, but it also experienced a significant reduction in thickness due to the high-impact energy. The aluminum facesheet did not bend because it was a relatively vital and rigid component of the sandwich structure. In the H6_STF and H6_STF_CNT (Fig. 10b–c) sandwich structures, the XPS foam core was disintegrated because it contained STFs or M-STFs that increased its viscosity and stiffness under impact. The STFs or M-STFs acted as solid-like materials that resisted the deformation and transferred the impact stress to the XPS foam core, causing it to crack and break. The aluminum facesheets did not deform because it was still a relatively strong and rigid component of the sandwich structure.

4. Conclusions

In this study, we studied the role of STF and M-STFs in the XPS foam core of a sandwich-structured composite with aluminum facesheets on reducing of force attenuation (FA) performance, which is crucial in impact protection applications. To add STF and M-STFs, six different geometries were designed and machined on the XPS core layer with the same amount of space (including cylindrical holes and rectangular channels with varying diameters and spacing between them). The study aimed to understand how FA can be affected in different XPS core geometries. Then, STF with 40 wt% SiO_2 in PEG was produced, and MWCNTs were added to STF up to 1.5 wt% to create M-STFs. The influence of MWCNTs on the electrical resistance of STF and the rheology of the fabricated suspensions was also investigated. According to the percolation threshold in the electrical resistance of M-STF (between 0.2 and 0.4), 0.5 wt% MWCNT was selected to be added to STF for M-STF-based sandwich structures. FA tests were performed at three different energy levels (5, 10, and 15 J) using a low-velocity impact system. The results showed that V6_STF and H6_STF sandwich structures had the best performance in FA reduction. Next, V6_STF and H6_STF sandwich structures were filled again with M-STF (0.5 wt% MWCNT) to study the effect of MWCNTs. The results showed that their FA performance improved by nearly 10% compared with V6_STF and H6_STF samples and 24.8% compared to the neat sandwich structure.

The results showed that including STFs and M-STFs in the core of sandwich structures could improve their anti-impact properties (in our case, FA performance). Moreover, the impact force direction was crucial to the STFs' performance. The results indicated that the V6_STF (in vertical-based designs) and H6_STF (in horizontal-based designs) sandwich structures showed the best performance in
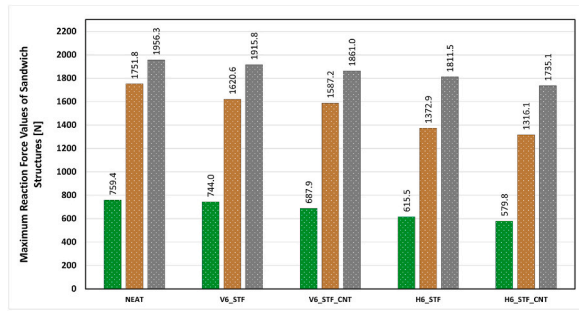
Fig. 8. Maximum reaction forces of designed sandwich structures filled with STF and M-STFs.
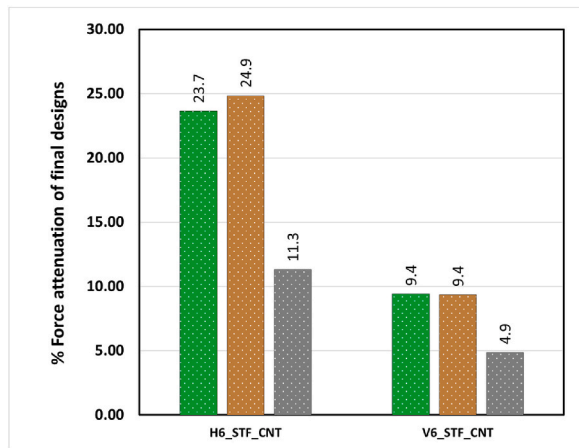

Fig. 9. Force attenuation performance of M-STF filled sandwich structures.
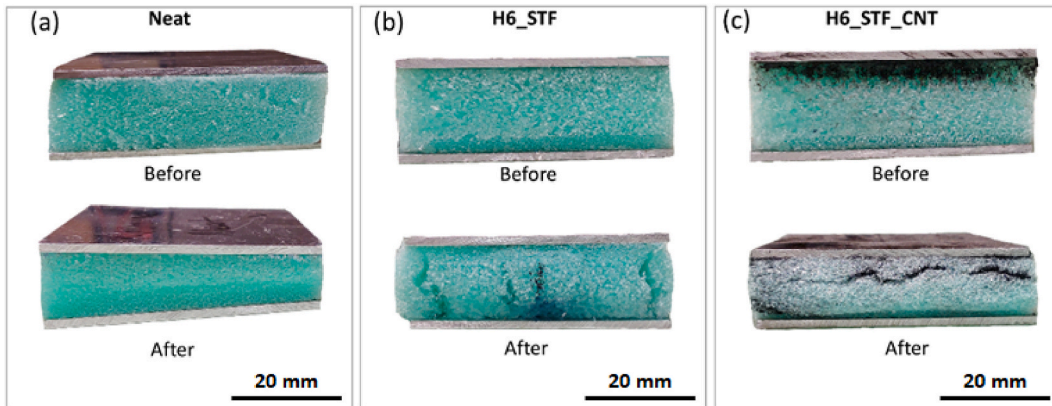

Fig. 10. Deformations before and after 15 J impact for (a) Neat, (b) H6_STF, and (c) H6_STF_CNT.

FA reduction. Additionally, adding MWCNTs to STFs further improved the FA performance in M-STF-filled sandwich structures (V6_STF_CNT and H6_STF_CNT). The findings of this study can be beneficial to engineering applications that require impact protection, EA, and vibration attenuation, such as military, transportation, and sports. Future research might focus on improving the composition and processing of STFs and M-STFs, establishing new methodologies and techniques for characterizing and predicting their behavior.

Data availability

The raw/processed data required to reproduce these findings cannot be shared at this time as the data also forms part of an ongoing

study.

CRediT authorship contribution statement

Mohammad Rauf Sheikhi: Writing – original draft, Formal analysis, Data curation. **Kenan Bayrak:** Writing – original draft, Investigation, Formal analysis. **Esra Ozdemir:** Writing – review & editing, Methodology, Conceptualization. **Selim Gürgen:** Writing – review & editing, Supervision, Project administration.

Declaration of competing interest

The authors declare that they have no known competing financial interests or personal relationships that could have appeared to influence the work reported in this paper.

Acknowledgements

References

[1] V. Birman, G.A. Kardomateas, Review of current trends in research and applications of sandwich structures, Compos. B Eng. 142 (2018) 221–240, https://doi.org/10.1016/j.compositesb.2018.01.027.

[2] W. Ma, R. Elkin, Sandwich Structural Composites, CRC Press, Boca Raton, 2021, https://doi.org/10.1201/9781003035374.

[3] J. Xiong, Y. Du, D. Mousanezhad, M. Eydani Asl, J. Norato, A. Vaziri, Sandwich structures with prismatic and foam cores: a review, Adv. Eng. Mater. 21 (2019), https://doi.org/10.1002/adem.201800036.

[4] A. Dogan, Low-velocity impact, bending, and compression response of carbon fiber/epoxy-based sandwich composites with different types of core materials, J. Sandw. Struct. Mater. 23 (2021) 1956–1971, https://doi.org/10.1177/1099636220908862.

[5] B. Vijaya Ramnath, K. Alagarraja, C. Elanchezhian, Review on sandwich composite and their applications, Mater. Today Proc. 16 (2019) 859–864, https://doi.org/10.1016/j.matpr.2019.05.169.

[6] F. Tarlochan, Sandwich structures for energy absorption applications: a review, Materials 14 (2021) 4731, https://doi.org/10.3390/ma14164731.

[7] R.F. Gibson, A review of recent research on mechanics of multifunctional composite materials and structures, Compos. Struct. 92 (2010) 2793–2810, https://doi.org/10.1016/j.compstruct.2010.05.003.

[8] A.D.B.L. Ferreira, P.R.O. Nóvoa, A.T. Marques, Multifunctional material systems: a state-of-the-art review, Compos. Struct. 151 (2016) 3–35, https://doi.org/10.1016/j.compstruct.2016.01.028.

[9] S. Gürgen, M.C. Kuşhan, W. Li, Shear thickening fluids in protective applications: a review, Prog. Polym. Sci. 75 (2017) 48–72, https://doi.org/10.1016/j.progpolymsci.2017.07.003.

[10] S. Gürgen (Ed.), Shear Thickening Fluid, Springer International Publishing, Cham, 2023, https://doi.org/10.1007/978-3-031-25717-9.

[11] M.R. Sheikhi, M. Hasanzadeh, Multi-phase shear thickening fluid, in: Shear Thickening Fluid, Springer International Publishing, Cham, 2023, pp. 33–51, https://doi.org/10.1007/978-3-031-25717-9_3.

[12] J. Qin, B. Guo, L. Zhang, T. Wang, G. Zhang, X. Shi, Soft armor materials constructed with Kevlar fabric and a novel shear thickening fluid, Compos. B Eng. 183 (2020) 107686, https://doi.org/10.1016/j.compositesb.2019.107686.

[13] K.L. White, H. Yao, X. Zhang, H.-J. Sue, Rheology of electrostatically tethered nanoplatelets and multi-walled carbon nanotubes in epoxy, Polymer (Guildf) 84 (2016) 223–233, https://doi.org/10.1016/j.polymer.2015.12.043.

[14] R.B. Ladani, S. Wu, A.J. Kinloch, K. Ghorbani, J. Zhang, A.P. Mouritz, C.H. Wang, Multifunctional properties of epoxy nanocomposites reinforced by aligned nanoscale carbon, Mater. Des. 94 (2016) 554–564, https://doi.org/10.1016/j.matdes.2016.01.052.

[15] X. Sha, K. Yu, H. Cao, K. Qian, Shear thickening behavior of nanoparticle suspensions with carbon nanofillers, J. Nanoparticle Res. 15 (2013) 1816, https://doi.org/10.1007/s11051-013-1816-x.

[16] S. Gürgen, M.C. Kuşhan, W. Li, The effect of carbide particle additives on rheology of shear thickening fluids, Korea-Australia Rheology, Journal 28 (2016) 121–128, https://doi.org/10.1007/s13367-016-0011-x.

[17] B. Seifried, F. Temelli, Viscosity and rheological behaviour of carbon dioxide-expanded fish oil triglycerides: measurement and modeling, J. Supercrit. Fluids 59 (2011) 27–35, https://doi.org/10.1016/j.supflu.2011.07.010.

[18] M.R. Sheikhi, M. Hasanzadeh, S. Gürgen, The role of conductive fillers on the rheological behavior and electrical conductivity of multi-functional shear thickening fluids (M-STFs), Adv. Powder Technol. 34 (2023) 104086, https://doi.org/10.1016/j.apt.2023.104086.

[19] S. Wang, S. Liu, J. Zhou, F. Li, J. Li, X. Cao, Z. Li, J. Zhang, B. Li, Y. Wang, X. Gong, Advanced triboelectric nanogenerator with multi-mode energy harvesting and anti-impact properties for smart glove and wearable e-textile, Nano Energy 78 (2020) 105291, https://doi.org/10.1016/j.nanoen.2020.105291.

[20] J. Zhang, Y. Wang, H. Deng, J. Zhou, S. Liu, J. Wu, M. Sang, X. Gong, A high anti-impact STF/Ecoflex composite structure with a sensing capacity for wearable design, Compos. B Eng. 233 (2022) 109656, https://doi.org/10.1016/j.compositesb.2022.109656.

[21] C. Zhao, X. Gong, S. Wang, W. Jiang, S. Xuan, Shear stiffening gels for intelligent anti-impact applications, Cell Rep Phys Sci 1 (2020) 100266, https://doi.org/10.1016/j.xcrp.2020.100266.

[22] P. Ying, W. Shen, Y. Xia, Shear stiffening gel under low-speed impact: mechanical behavior characterization and protective performance analysis, Mater. Des. 231 (2023) 112047, https://doi.org/10.1016/j.matdes.2023.112047.

[23] M.R. Sheikhi, S. Gürgen, Intelligent polymers for multi-functional applications: mechanical and electrical aspects, Polymers 15 (2023) 2620, https://doi.org/10.3390/polym15122620.

[24] S. Gürgen, M.C. Kuşhan, The ballistic performance of aramid based fabrics impregnated with multi-phase shear thickening fluids, Polym. Test. 64 (2017) 296–306, https://doi.org/10.1016/j.polymertesting.2017.11.003.

[25] K. Fu, H. Wang, L. Chang, M. Foley, K. Friedrich, L. Ye, Low-velocity impact behaviour of a shear thickening fluid (STF) and STF-filled sandwich composite panels, Compos. Sci. Technol. 165 (2018) 74–83, https://doi.org/10.1016/j.compscitech.2018.06.013.

[26] M. Bajya, A. Majumdar, B.S. Butola, S.K. Verma, D. Bhattacharjee, Design strategy for optimising weight and ballistic performance of soft body armour reinforced with shear thickening fluid, Compos. B Eng. 183 (2020) 107721, https://doi.org/10.1016/j.compositesb.2019.107721.

[27] N.A. Bhalla, Shear thickening fluid-based protective structures against high velocity impacts, in: Shear Thickening Fluid, Springer International Publishing, Cham, 2023, pp. 139–152, https://doi.org/10.1007/978-3-031-25717-9_8.

[28] M.R. Sheikhi, S. Gürgen, Deceleration behavior of multi-layer cork composites intercalated with a non-Newtonian material, Arch. Civ. Mech. Eng. 23 (2022) 2, https://doi.org/10.1007/s43452-022-00544-z.

[29] M.R. Sheikhi, S. Gürgen, Anti-impact design of multi-layer composites enhanced by shear thickening fluid, Compos. Struct. 279 (2022) 114797, https://doi.org/10.1016/j.compstruct.2021.114797.

[30] Ö. Yay, M.R. Sheikhi, G. Kunt, S. Gürgen, Shock absorption in shear-thickening fluid included 3D-printed structures, in: Shear Thickening Fluids in Protective Applications, Springer Nature Switzerland, Cham, 2024, pp. 27–38, https://doi.org/10.1007/978-3-031-42951-4_4.

[31] M.R. Sheikhi, T. Türkistanlı, N.S. Akşit, S. Gürgen, Deceleration behavior of shear-thickening fluid impregnated foams under low-velocity impact, in: Shear Thickening Fluids in Protective Applications, Springer Nature Switzerland, Cham, 2024, pp. 17–25, https://doi.org/10.1007/978-3-031-42951-4_3.

[32] X. Gong, Y. Xu, W. Zhu, S. Xuan, W. Jiang, W. Jiang, Study of the knife stab and puncture-resistant performance for shear thickening fluid enhanced fabric, J. Compos. Mater. 48 (2014) 641–657, https://doi.org/10.1177/0021998313476525.

[33] S. Gürgen, M.C. Kuşhan, The stab resistance of fabrics impregnated with shear thickening fluids including various particle size of additives, Compos Part A Appl Sci Manuf 94 (2017) 50–60, https://doi.org/10.1016/j.compositesa.2016.12.019.

[34] M.R. Sheikhi, Ö. Yay, M.C. Kuşhan, Penetration resistance of high-performance textiles treated with CNT-reinforced STF, in: Shear Thickening Fluids in Protective Applications, Springer Nature Switzerland, Cham, 2024, pp. 3–16, https://doi.org/10.1007/978-3-031-42951-4_2.

[35] K. Liu, C.-F. Cheng, L. Zhou, F. Zou, W. Liang, M. Wang, Y. Zhu, A shear thickening fluid based impact resistant electrolyte for safe Li-ion batteries, J. Power Sources 423 (2019) 297–304, https://doi.org/10.1016/j.jpowsour.2019.03.056.

[36] G.M. Veith, B.L. Armstrong, H. Wang, S. Kalnaus, W.E. Tenhaeff, M.L. Patterson, Shear thickening electrolytes for high impact resistant batteries, ACS Energy Lett. 2 (2017) 2084–2088, https://doi.org/10.1021/acsenergylett.7b00511.

[37] M.R. Sheikhi, S. Gürgen, M.C. Kuşhan, Shear thickening fluid in spall-liner applications, in: Advances in Healthcare and Protective Textiles, Elsevier, 2023, pp. 487–508, https://doi.org/10.1016/B978-0-323-91188-7.00002-9.

[38] M.R. Sheikhi, M. Hasanzadeh, Blast protection with shear-thickening fluid-integrated composites, in: Shear Thickening Fluids in Protective Applications, Springer Nature Switzerland, Cham, 2024, pp. 89–102, https://doi.org/10.1007/978-3-031-42951-4_7.

[39] Q. Zhao, J. Yuan, H. Jiang, H. Yao, B. Wen, Vibration control of a rotor system by shear thickening fluid dampers, J. Sound Vib. 494 (2021) 115883, https://doi.org/10.1016/j.jsv.2020.115883.

[40] M. Wei, G. Hu, L. Li, H. Liu, Development and theoretically evaluation of an STF–SF isolator for seismic protection of structures, Meccanica 53 (2018) 841–856, https://doi.org/10.1007/s11012-017-0785-z.

[41] M. Rauf Sheikhi, S. Gürgen, J. Li, M. Alper Sofuoğlu, M. Hasanzadeh, M. Cemal Kuşhan, Z. Chen, Design of smart sandwich structures enhanced by multi-functional shear thickening fluids (M−STFs): anti-vibration and electrical conductivity, Compos. Struct. 324 (2023) 117520, https://doi.org/10.1016/j.compstruct.2023.117520.

[42] M.R. Sheikhi, S. Gürgen, M.C. Kuşhan, Vibration damping systems with shear thickening fluid, in: Shear Thickening Fluid, Springer International Publishing, Cham, 2023, pp. 77–97, https://doi.org/10.1007/978-3-031-25717-9_5.

[43] S. Gürgen, M.A. Sofuoğlu, Vibration attenuation of sandwich structures filled with shear thickening fluids, Compos. B Eng. 186 (2020) 107831, https://doi.org/10.1016/j.compositesb.2020.107831.

[44] S. Gürgen, M.A. Sofuoğlu, Smart polymer integrated cork composites for enhanced vibration damping properties, Compos. Struct. 258 (2021) 113200, https://doi.org/10.1016/j.compstruct.2020.113200.

[45] M.R. Sheikhi, M.A. Sofuoğlu, Z. Chen, Shear thickening fluid integrated sandwich structures for vibration isolation, in: Shear Thickening Fluid, Springer International Publishing, Cham, 2023, pp. 27–40, https://doi.org/10.1007/978-3-031-35521-9_3.

[46] C. Fischer, S.A. Braun, P.-E. Bourban, V. Michaud, C.J.G. Plummer, J.-A.E. Månson, Dynamic properties of sandwich structures with integrated shear-thickening fluids, Smart Mater. Struct. 15 (2006) 1467–1475, https://doi.org/10.1088/0964-1726/15/5/036.

[47] J. Lim, S.-W. Kim, Enhanced damping characteristics of carbon fiber reinforced polymer–based shear thickening fluid hybrid composite structures, J. Intell. Mater. Syst. Struct. 31 (2020) 2291–2303, https://doi.org/10.1177/1045389X19898769.

[48] S. Gürgen, M.A. Sofuoğlu, Experimental investigation on vibration characteristics of shear thickening fluid filled CFRP tubes, Compos. Struct. 226 (2019) 111236, https://doi.org/10.1016/j.compstruct.2019.111236.

[49] Z. Man, L. Chang, Shear thickening fluid in surface finishing operations, in: Shear Thickening Fluid, Springer International Publishing, Cham, 2023, pp. 99–114, https://doi.org/10.1007/978-3-031-25717-9_6.

[50] M. Li, B. Lyu, J. Yuan, W. Yao, F. Zhou, M. Zhong, Evolution and equivalent control law of surface roughness in shear-thickening polishing, Int. J. Mach. Tool Manufact. 108 (2016) 113–126, https://doi.org/10.1016/j.ijmachtools.2016.06.007.

[51] S. Gürgen, M.A. Sofuoğlu, Integration of shear thickening fluid into cutting tools for improved turning operations, J. Manuf. Process. 56 (2020) 1146–1154, https://doi.org/10.1016/j.jmapro.2020.06.012.

[52] F. Zhao, L. Wu, Z. Lu, J.-H. Lin, Q. Jiang, Design of shear thickening fluid/polyurethane foam skeleton sandwich composite based on non-Newtonian fluid solid interaction under low-velocity impact, Mater. Des. 213 (2022) 110375, https://doi.org/10.1016/j.matdes.2021.110375.

[53] C. Caglayan, I. Osken, A. Ataalp, H.S. Turkmen, H. Cebeci, Impact response of shear thickening fluid filled polyurethane foam core sandwich composites, Compos. Struct. 243 (2020) 112171, https://doi.org/10.1016/j.compstruct.2020.112171.

[54] X. Wu, K. Xiao, Q. Yin, F. Zhong, C. Huang, Experimental study on dynamic compressive behaviour of sandwich panel with shear thickening fluid filled pyramidal lattice truss core, Int. J. Mech. Sci. 138–139 (2018) 467–475, https://doi.org/10.1016/j.ijmecsci.2018.02.029.

[55] V.A. Chatterjee, S.K. Verma, D. Bhattacharjee, I. Biswas, S. Neogi, Enhancement of energy absorption by incorporation of shear thickening fluids in 3D-mat sandwich composite panels upon ballistic impact, Compos. Struct. 225 (2019) 111148, https://doi.org/10.1016/j.compstruct.2019.111148.

[56] S. Gürgen, F.A.O. Fernandes, R.J.A. de Sousa, M.C. Kuşhan, Development of eco-friendly shock-absorbing cork composites enhanced by a non-Newtonian fluid, Appl. Compos. Mater. 28 (2021) 165–179, https://doi.org/10.1007/s10443-020-09859-7.

[57] T. Ghoshal, P.R. Parmar, T. Bhuyan, D. Bandyopadhyay, Polystyrene Foams: Materials, Technology, and Applications, 2023, pp. 121–141, https://doi.org/10.1021/bk-2023-1439.ch006.

[58] M.R. Sheikhi, M. Hasanzadeh, S. Gürgen, J. Li, Enhanced anti-impact resistance of polyurethane foam composites with multi-phase shear thickening fluids containing various carbon nanofillers, Mater. Today Commun. 38 (2024) 107991, https://doi.org/10.1016/j.mtcomm.2023.107991.

[59] C.H. Lau, R. Cervini, S.R. Clarke, M.G. Markovic, J.G. Matisons, S.C. Hawkins, C.P. Huynh, G.P. Simon, The effect of functionalization on structure and electrical conductivity of multi-walled carbon nanotubes, J. Nanoparticle Res. 10 (2008) 77–88, https://doi.org/10.1007/s11051-008-9376-1.

[60] M. Wei, Y. Lv, L. Sun, H. Sun, Rheological properties of multi-walled carbon nanotubes/silica shear thickening fluid suspensions, Colloid Polym. Sci. 298 (2020) 243–250, https://doi.org/10.1007/s00396-020-04599-3.

[61] N.A. Mohd Radzuan, A.B. Sulong, J. Sahari, A review of electrical conductivity models for conductive polymer composite, Int. J. Hydrogen Energy 42 (2017) 9262–9273, https://doi.org/10.1016/j.ijhydene.2016.03.045.

[62] Q. Xue, J. Sun, Electrical conductivity and percolation behavior of polymer nanocomposites, in: Polymer Nanocomposites, Springer International Publishing, Cham, 2016, pp. 51–82, https://doi.org/10.1007/978-3-319-28238-1_3.